HHS Public Access

Author manuscript

Proc SPIE Int Soc Opt Eng. Author manuscript; available in PMC 2015 June 15.

Published in final edited form as:

Proc SPIE Int Soc Opt Eng. 2015 March 17; 9417: . doi:10.1117/12.2081859.

Validation of CBCT for the computation of textural biomarkers

Beatriz Paniagua[1], **Antonio Carlos Ruellas**[2,5], **Erika Benavides**[2], **Steve Marron**[3], **Larry Woldford**[4], and **Lucia Cevidanes**[2]

[1]University of North Carolina at Chapel Hill, Departments of Psychiatry, Computer Science and Orthodontics

[2]University of Michigan, School of Dentistry

[3]University of North Carolina at Chapel Hill, Department of Statistics and Operational Research

[4]Texas A&M Health Science Center, Baylor College of Dentistry

[5]Federal University of Rio de Janeiro, School of Dentistry

Abstract

Osteoarthritis (OA) is associated with significant pain and 42.6% of patients with TMJ disorders present with evidence of TMJ OA. However, OA diagnosis and treatment remain controversial, since there are no clear symptoms of the disease. The subchondral bone in the TMJ is believed to play a major role in the progression of OA. We hypothesize that the textural imaging biomarkers computed in high resolution Conebeam CT (hr-CBCT) and μCT scans are comparable. The purpose of this study is to test the feasibility of computing textural imaging biomarkers in-vivo using hr-CBCT, compared to those computed in μCT scans as our Gold Standard. Specimens of condylar bones obtained from condylectomies were scanned using μCT and hr-CBCT. Nine different textural imaging biomarkers (four co-occurrence features and five run-length features) from each pair of μCT and hr-CBCT were computed and compared. Pearson correlation coefficients were computed to compare textural biomarkers values of μCT and hr-CBCT. Four of the nine computed textural biomarkers showed a strong positive correlation between biomarkers computed in μCT and hr-CBCT. Higher correlations in Energy and Contrast, and in GLN (grey-level non-uniformity) and RLN (run length non-uniformity) indicate quantitative texture features can be computed reliably in hr-CBCT, when compared with μCT. The textural imaging biomarkers computed in-vivo hr-CBCT have captured the structure, patterns, contrast between neighboring regions and uniformity of healthy and/or pathologic subchondral bone. The ability to quantify bone texture non-invasively now makes it possible to evaluate the progression of subchondral bone alterations, in TMJ OA.

Keywords

Temporomandibular joint; Osteoarthritis; subchondral bone; texture analysis

INTRODUCTION

Osteoarthritis (OA), the most prevalent arthritis worldwide, is associated with significant pain and disability and affects 13.9% of adults at any given time[1,2]. Of these conditions,

disorders of the temporomandibular joint (TMJ) result in $4 billion annual health care costs in the US. According to recently revised TMJ imaging criteria, 42.6% of patients with TMJ disorders presented with evidence of TMJ OA[2]. However, diagnosis and treatment of these conditions remain controversial. To date, there is no single sign, symptom, or test that can clearly diagnose early stages of OA. Instead, the diagnosis is based on a consideration of several factors, including the presence of characteristic symptoms of osteoarthritis (pain, mobility problems, etc), results of laboratory tests and radiological tests.

The bone in the TMJ condyle is the site of numerous dynamic morphological transformations, which are an integral part of the initiation/progression of OA, not merely secondary manifestations to cartilage degradation. Specifically, the subchondral bone also seems to play a significant role. Recent work to evaluate subchondral bone and structure have been focused in analyzing textural features and bone density/volume in two-dimensional (2D) radiographs[3–5], and 3D imaging modalities such as Computed Tomography (CT)[6,7]. Volumetric analyses cannot detect structural changes at specific locations, and they lack the ability to quantify subtle gray-level variations within the low-density bone three-dimensional structure. 2D texture analysis is not an appropriate method to analyze subchondral bone texture either, since subchondral trabecular bone architecture is highly anisotropic; that is, the trabeculae are oriented in different directions, and the mechanical properties of the tissue are therefore different in the different planes. Hence, 3D texture analysis is the only way to capture the complex structure of the subchondral bone.

Comparisons of μCT (using the Radon transform[8]) and CBCT (using the Feldkamp algorithm[9], that introduces an averaging-blur effect to minimize artifacts of cone-beam imaging) have been recently reported for dental implant sites in cadavers[10] and for assessments of bone quality in femurs obtained from animal models[11]. In conclusion, very little work exists in methods that explore the 3D nature of subchondral texture, and all of them use CT as image modality.

It is important to highlight that CT is an imaging modality that provides great bony tissue contrast, but to the cost of a higher radiation dose for the patient. Specifically, micro-CT (μCT) is a CT machine that acquires images at a very high resolution and the preferred imaging modality for animal studies, where the sizes of the cross-sections are in the micrometer range[12]. Due to the high radiation doses, micro-CT is not a good choice of imaging modality in living patients. Recently high resolution CBCT (hr-CBCT) scanner[13] can now acquire images of the craniofacial complex that allow qualitative and quantitative assessments of both hard tissue subtle spread of contrast, without the higher cost of radiation for the patient. These images display a high degree of clarity compared to classical CBCT and enable comprehensive examination for diagnosing of bone lesions such as dental root apical lesions and subchondral bone cysts.

The purpose of this study was to demonstrate that it is possible to compute textural imaging biomarkers using hr-CBCT. For that we compared textural imaging biomarkers computed in hr-CBCT to the same biomarkers computed in μCT scans as our Gold Standard. Our hypothesis was that the textural imaging biomarkers obtained for each modality would be comparable, demonstrating the accuracy to detect textural features in subchondral bone of

hr-CBCT. This work is crucial to justify the usage of hr-CBCT in OA patients, for the quantitative evaluation of the structure of the subchondral bone, as an early marker of OA.

MATERIALS

We used 16 specimens of condylar bones obtained from condylectomies that were scanned using μCT and hr-CBCT. The present population consisted in females with ages ranging from 18 to 64 years old.

For μCT[14] (μCT100 Scanco Medical, Bassersdorf, Switzerland) image acquisition specimens were embedded in 1% agarose and placed in a 34 mm diameter tube and scanned over the entire length of the sample. Scan settings were: voxel size 34.4 μm, 90 kVp, 155 μA, medium resolution, 0.5 mm AL filter, and integration time 500 ms. For hr-CBCT (3D Accuitomo, J Morita MFG Corp, Kyoto Japan) scan settings were: voxel size 80 μm, 90 kVp, 1 mA, field of view 40x40.

Segmentation for all bony samples obtained from μCT and CBCT structures was performed semi-automatically using the user interactive InsightSNAP program[15]. Three-dimensional virtual models of the condyles and trabeculae for each sample were built (see figure 1) using 3DSlicer software[16] from a set of approximately 500 axial cross-sectional slices for each image, with the voxels reformatted to an isotropic of $0.08 \times 0.08 \times 0.08 mm^3$.

METHODS

μCT and hr-CBCT and scans are registered to each other using a two-step registration. First, scans, segmentations and 3d virtual models were manually approximated via rigid transformation using 3DSlicer[16]. Next, we used a fully automated voxel-wise registration to align each μCT scan to its correspondent hr-CBCT scan using CMFRegistration tool[17] in 3DSlicer.

After registration, two sets of 3D textural features were computed on each pair of μCT and hr-CBCT for each bony sample.

1. Co-occurrence features – This set of descriptors designed initially by Haralick *et al.*[18] are computed from a grey-level co-occurrence matrix (GLCM) that is a matrix defined over an image to express the distribution of co-occurring grey intensity values at a given direction. For our study, four features were computed: Entropy, Energy, Contrast and Homogeneity.
    a. Entropy is a feature that expresses the level of organization of a texture. A completely random distribution of grey-level intensities in the trabecular bone would have very high entropy, while an image with the same grey-level across all voxels would have very low value of entropy.
    b. Energy is a feature that measures of local uniformity of texture. The higher the energy value, the bigger the uniformity and organization of the texture.
    c. Contrast is a feature that measures local grey-level variation in the GLCM matrix. If the neighboring pixels in the texture are very similar in their grey-

level values then the contrast in the image is very low. Contrast is 0 for a constant image.

d. Homogeneity is a feature that measures the uniformity of the non-zero entries in the GLCM. If the texture contains repetitive structures, homogeneity will be high, for patterns with a big variation in texture elements and spatial arrangements homogeneity will be low.

2. Run-length features – This set of descriptors are based in run lengths computed in a texture[19]. A grey-level run is a set of consecutive, collinear picture points having the same grey-level value. The length of the run is the number of picture points in the run. For a given picture, we can compute a grey-level run length matrix (GLRLM) for runs having any given direction. For our study, five features were computed: short run emphasis (SRE), long run emphasis (LRE), grey-level non-uniformity (GLN), run length non-uniformity (RLN) and run percentage (RP).

a. SRE measures the distribution of short runs. SRE is expected large for fine textures.

b. LRE is a feature that measures distribution of long runs. LRE is highly is expected large for coarse structural textures

c. GLN measures the similarity of grey-level values through out the texture. The GLN is expected small if the grey-level values are alike through out the whole texture.

a. RLN is a feature that measures the similarity of the length of runs through out the image. The RLN is expected small if the run lengths are alike through out the image.

a. RP is a feature ratio of the total number of runs to the total number of possible runs if all runs had a length of one. It should have its lowest value for pictures with the most linear structure.

RESULTS

We computed our 9 textural features for each pair of μCT and hr-CBCT, and calculated the Pearson product-moment correlation coefficient (r) between the textural values of μCT and textural values of hr-CBCT. Correlation results for co-ocurrence and run-length textural features are described in Tables 1 and 2.

Table 1 displays higher positive correlation between μCT and hr-CBCT computed descriptors for energy and contrast features. Higher correlation rates in Energy and Contrast indicate that both the uniform tiny lattice-shaped spicules that form the subchondral bone (measured by Energy) and also the differences between tissue signal intensities (Contrast) can be measured reliably both in μCT and hr-CBCT.

Figure 2a and 2b display scatterplots for both Energy and Contrast. A marked positive correlation can be observed for both textural features. When looking at two representative samples of each graph, i.e. minimum and maximum values of Entropy and Contrast for both

μCT and hr-CBCT, we can see that these two features capture important textural characteristics. 5R is a sample with a lot of dense cortical bone, which does not have the same repetitive textural patterns and different grey-level intensities, and that is why low values are found for both features. On the other hand, both samples 10R and 3R display lots of lattice-shaped patterns and high contrast edges, which explains both the high Energy values in 13R, and Contrast values in 10R.

Table 2 displays higher positive correlation between μCT and hr-CBCT computed textural descriptors for GLN (grey-level non-uniformity) and RLN (run length non-uniformity). Higher correlation rates in GLN and RLN indicate that both the gray-level distributions (GLN) and the size of areas of same gray-level (RLN) can be measured reliably both in μCT and hr-CBCT.

Figure 3a and 3b display scatterplots for GLN and RLN. A marked positive correlation can be observed. When doing the same observation than for Figure 6, by looking at two representative samples of each graph, we can see that important textural characteristics are captured by these two features. 5R has lower GLN and RLN values, due to the fact grey-level values and run-lengths are alike through out the sample, while 10R has higher values due to the heterogeneity of both grey-levels and sizes of areas of the same grey-level.

DISCUSSION

In TMJ OA, a strong scientific rationale exists for looking into full joint biomarkers, shifting the focus in OA from articular cartilage to subchondral bone changes. The subchondral bone in the TMJ condyle is the site of numerous dynamic morphological transformations, which are part of the initiation/progression of OA, not merely secondary manifestations to cartilage degradation. The appearance of subchondral cysts and trabecular density loss (see figure 4) can be associated with the progression of OA.

In fact, texture differences due to pathology in the subchondral bone can be easily perceived with the naked-eye in scans obtained with an appropriate image modality, such as the proposed hr-CBCT. Figure 5 shows the clear differences between one single patient with TMJ OA and a healthy subject. There are clear pathological textural features of the trabecular structure in the patient with TMJ OA, such as areas of bone loss with increased patches of low gray-level values (bone loss shows as dark spots in the scan) or decreased number of areas of with small trabecular lattices.

This illustrates that hr-CBCT images provide qualitative and quantitative evaluation of the hard tissue displaying better contrast and resolution compared to classical CBCT (Figure 6). With the work presented in this manuscript, we have demonstrated that hr-CBCT can capture subchondral texture in a reliable way, as compared with μCT as our Gold Standard.

Our results show that four of our nine textural features computed in both μCT and hr-CBCT demonstrated that hr-CBCT has the potential of accurately represent texture in-vivo patients. Textural characteristics in hr-CBCT have the ability of capturing structure, patterns, contrast between neighboring regions and uniformity of subchondral texture. To our knowledge this is the first study to look at subchondral bone texture in 3D. Our research team has used

CBCT images to characterize cortical bone remodeling in TMJ OA in the past[20–23]; however, the greater noise observed in conventional CBCT imaging of low density bone has limited our ability to study subchondral bone texture (see figure 6a). Classical CBCT scan resolutions and noise were enough to reconstruct cortical bone, but are insufficient to accurately represent subchondral bone texture, but since recently high resolution CBCT (hr-CBCT) scanners[13] can acquire images of the craniofacial complex that allow qualitative and quantitative assessments of hard tissue with subtle spread of contrast (see figure 6b).

Literature exploring the nature of subchondral texture in OA lacks studies that look at co-occurrence or run-length features. However, it is possible to find previous results comparing volumetric markers in μCT and CBCT[10,11], but as described before volumetric markers lack the ability to capture the 3D structure of bone trabecula. Preliminary work, using the proposed features to examine muscle texture in MRI[24,25], has shown that co-occurrence or run-length features detect pathology associated with diseases affecting muscular texture.

As future work, we plan to use the validated 3D texture biomarkers to quantify bone texture phenotypes that may identify patients at risk for further bone destruction. Quantitative analysis of subchondral bony changes may decrease the controversial treatment protocols assessing treatment effectiveness in future clinical trials. The knowledge gained from this type of analysis will allow more rational clinical decision making for patients with TMJ OA, and also be applicable to research on OA in other joints.

REFERENCES

1. Hussain AM, Packota G, Major PW, Flores-Mir C. Myhrvold N. Role of different imaging modalities in assessment of temporomandibular joint erosions and osteophytes: a systematic review. Dentomaxillofac. Radiol. 2008; 37(2):63–71. "Confessions of a cybershaman," Slate, 12 June 1997, http://www.slate.com/CriticalMass/97-06-12/CriticalMass.asp (19 October 1997). [PubMed: 18239033]
2. CDC. Arthritis - Data and Statistics. CDC. 2014 Aug 27. http://www.cdc.gov/arthritis/data_statistics.htm (27 August 2014).
3. Wong AKO, Beattie KA, Emond PD, Inglis D, Duryea J, Doan A, Ioannidis G, Webber CE, O'Neill J, et al. Quantitative analysis of subchondral sclerosis of the tibia by bone texture parameters in knee radiographs: site-specific relationships with joint space width. Osteoarthritis Cartilage. 2009; 17(11):1453–1460. [PubMed: 19481622]
4. Wolski M, Podsiadlo P, Stachowiak GW, Lohmander LS, Englund M. Differences in trabecular bone texture between knees with and without radiographic osteoarthritis detected by directional fractal signature method. Osteoarthritis Cartilage. 2010; 18(5):684–690. [PubMed: 20175970]
5. Blumenkrantz G, Stahl R, Carballido-Gamio J, Zhao S, Lu Y, Munoz T, Hellio Le Graverand-Gastineau M-P, Jain SK, Link TM, et al. The feasibility of characterizing the spatial distribution of cartilage T(2) using texture analysis. Osteoarthritis Cartilage. 2008; 16(5):584–590. [PubMed: 18337129]
6. Urish KL, Keffalas MG, Durkin JR, Miller DJ, Chu CR, Mosher TJ. T2 texture index of cartilage can predict early symptomatic OA progression: data from the osteoarthritis initiative. Osteoarthritis Cartilage. 2013; 21(10):1550–1557. [PubMed: 23774471]
7. Bousson V, Lowitz T, Laouisset L, Engelke K LJ. CT imaging for the investigation of subchondral bone in knee osteoarthritis. Osteoporos. Int. 2012; 23(Supplemental 8):861–865. [PubMed: 22120910]
8. Radon J. On the Determination of Functions from Their Integral Values along Certain Manifolds. IEEE Trans. Med. Imaging. 1986; 5(4):170–176. [PubMed: 18244009]

9. Feldkamp LA, Davis LC, Kress JW. Practical cone-beam algorithm. J. Opt. Soc. Am. A. 1984; 1(6): 612.
10. Ibrahim N, Parsa A, Hassan B, van der Stelt P, Aartman IHA, Wismeijer D. Accuracy of trabecular bone microstructural measurement at planned dental implant sites using cone-beam CT datasets. Clin. Oral Implants Res. 2014; 25(8):941–945. [PubMed: 23581278]
11. Wang T, Wen C-Y, Yan C-H, Lu W-W, Chiu K-Y. Spatial and temporal changes of subchondral bone proceed to microscopic articular cartilage degeneration in guinea pigs with spontaneous osteoarthritis. Osteoarthritis Cartilage. 2013; 21(4):574–581. [PubMed: 23313833]
12. U. N. L. of M. M. S. H. X-Ray Microtomography. MeSH. 2014 Aug 28. http://www.nlm.nih.gov/cgi/mesh/2011/MB_cgi?mode=&term=X-Ray+Microtomography (28 August 2014).
13. Morita Kyoto Japan. Accuitomo. 2014 Sep 25. http://www.morita.com/usa/cms/website.php?id=/en/products/dental/diagnostic_and_imaging_equipment/3d_accuitomo_170.html (25 September 2014).
14. University of Michigan School of Dentistry micro CT Core, funded in part by NIH/NCRR S10RR026475-01.
15. Yushkevich PA, Piven J, Hazlett HC, Smith RG, Ho S, Gee JC, Gerig G. User-guided 3D active contour segmentation of anatomical structures: significantly improved efficiency and reliability. Neuroimage. 2006; 31(3):1116–1128. [PubMed: 16545965]
16. 3DSlicer. 2015 Jan 22. www.slicer.org (22 January 2015).
17. CMFReg. 2015 Jan 22. http://www.slicer.org/slicerWiki/index.php/Documentation/Nightly/Extensions/CMFreg (22 January 2015).
18. Haralick RM, Shanmugam K, Dinstein I. Textural Features for Image Classification. IEEE Trans. Syst. Man. Cybern. 1973; 3(6):610–621. IEEE.
19. Galloway MM. Texture analysis using gray level run lengths. Comput. Graph. Image Process. 1975; 4(2):172–179.
20. Cevidanes LHS, Hajati a-K, Paniagua B, Lim PF, Walker DG, Palconet G, Nackley aG, Styner M, Ludlow JB, et al. Quantification of condylar resorption in temporomandibular joint osteoarthritis. Oral Surg. Oral Med. Oral Pathol. Oral Radiol. Endod. 2010; 110(1):110–117. Elsevier Inc. [PubMed: 20382043]
21. Paniagua B, Cevidanes L, Walker D, Zhu H, Guo R, Styner M. Clinical application of SPHARM-PDM to quantify temporomandibular joint osteoarthritis. Comput. Med. Imaging Graph. 2011; 35(5):345–352. Elsevier Ltd. [PubMed: 21185694]
22. Schilling J, Gomes LCR, Benavides E, Nguyen T, Paniagua B, Styner M, Boen V, Gonçalves JR, Cevidanes LHS. Regional 3D superimposition to assess temporomandibular joint condylar morphology. Dentomaxillofac. Radiol. 2014; 43(1):20130273. [PubMed: 24170802]
23. Goncalves JR, Wolford LM, Cassano DS, da Porciuncula G, Paniagua B, Cevidanes LH. Temporomandibular joint condylar changes following maxillomandibular advancement and articular disc repositioning. J. Oral Maxillofac. Surg. 2013; 71(10):1759.e1–1759.e15. [PubMed: 24040949]
24. Wang J, Fan Z, Vandenborne K, Walter G, Shiloh-Malawsky Y, An H, Kornegay JN, Styner MA. A computerized MRI biomarker quantification scheme for a canine model of Duchenne muscular dystrophy. Int. J. Comput. Assist. Radiol. Surg. 2013; 8(5):763–774. [PubMed: 23299128]
25. Fan Z, Wang J, Ahn M, Shiloh-Malawsky Y, Chahin N, Elmore S, Bagnell CR, Wilber K, An H, et al. Characteristics of magnetic resonance imaging biomarkers in a natural history study of golden retriever muscular dystrophy. Neuromuscul. Disord. 2014; 24(2):178–191. [PubMed: 24295811]

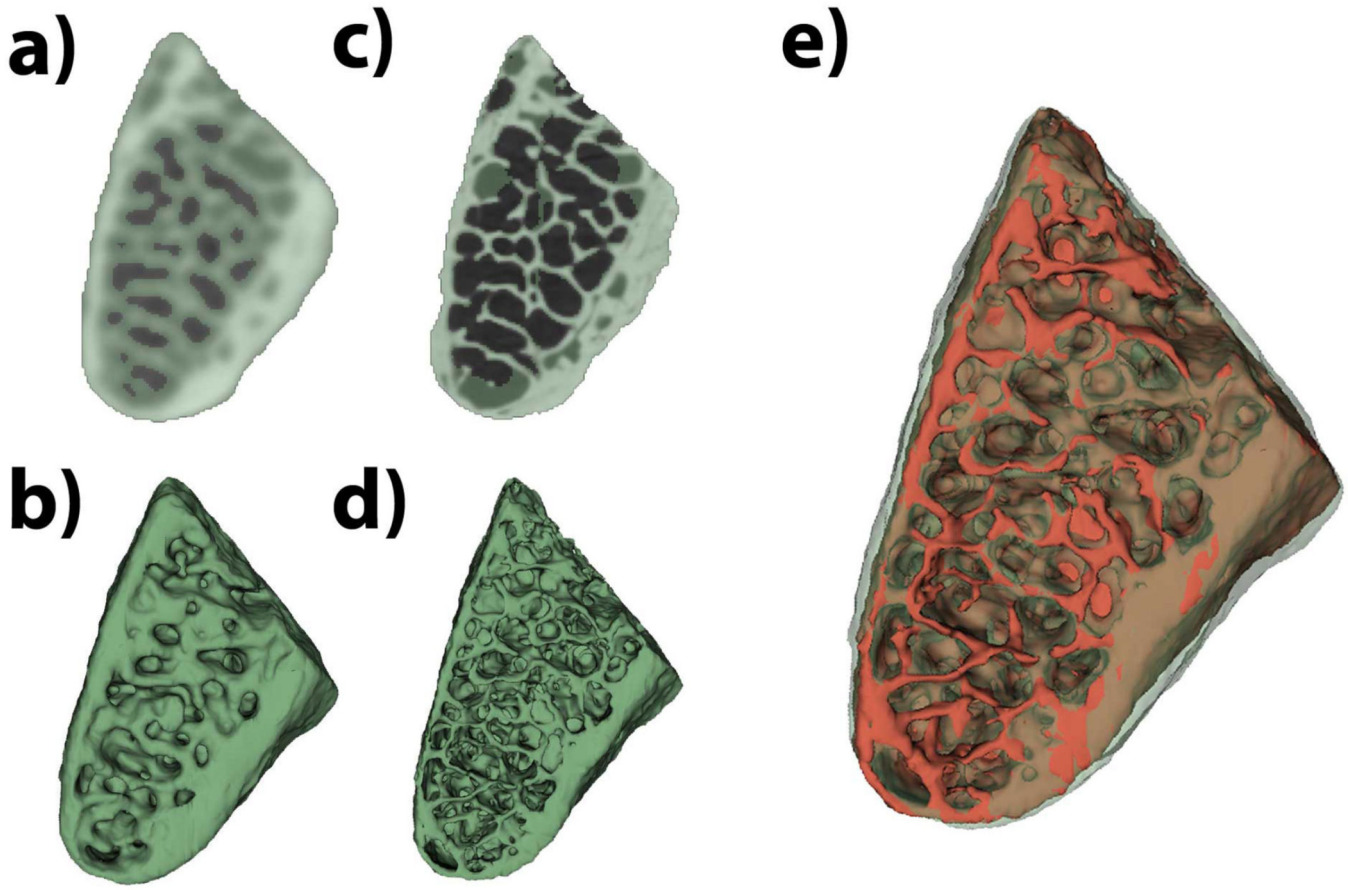

Figure 1.
3D segmentations and virtual models for hr-CBCT (a and b, respectively) and μCT (c and d, respectively) e) 3D virtual models for hr-CBCT (green semitransparent) and μCT (red solid) compared.

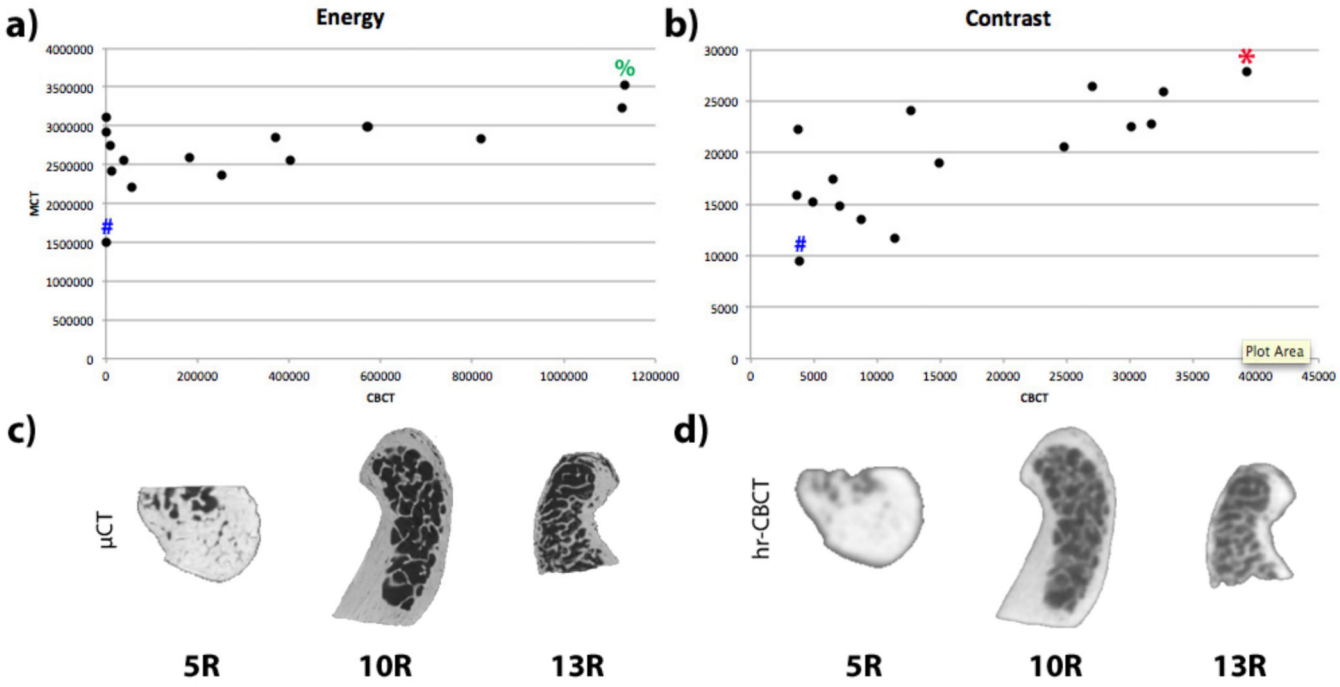

Figure 2.

Scatterplots for a) Energy and b) Contrast. Visualization of bony samples 5R, 10R and 13R for c) µCT and d) hr-CBCT. Blue (#) sign in both a) and b) show results for the sample 5R. Green (%) sign in a) show results for the sample 13R. Red (*) sign in b) show results for the sample 10R.

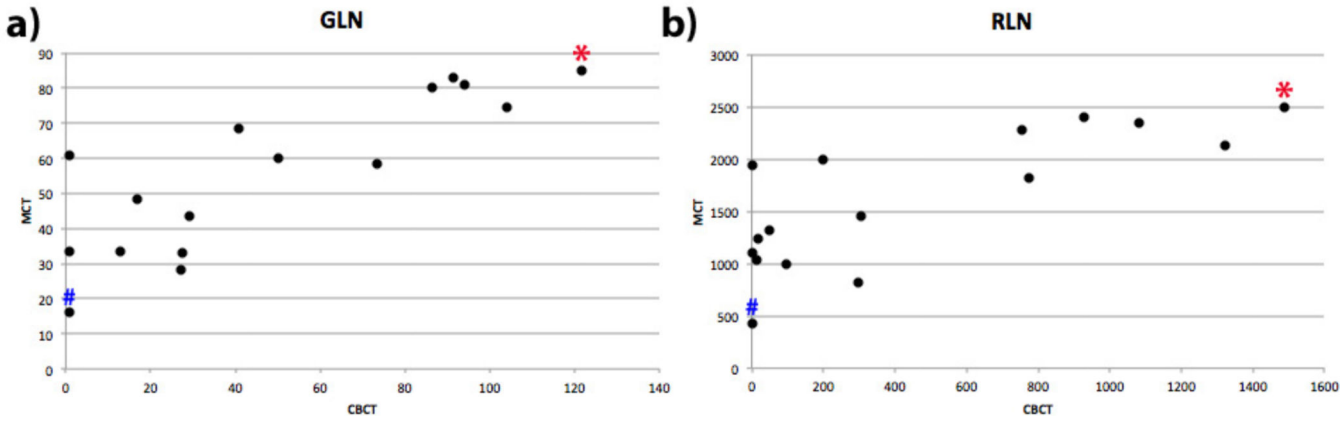

Figure 3.

Scatterplots for a) GLN and b) RLN. Blue (#) sign in both a) and b) show results for the sample 5R. Red (*) sign in both a) and b) show results for the sample 10R.

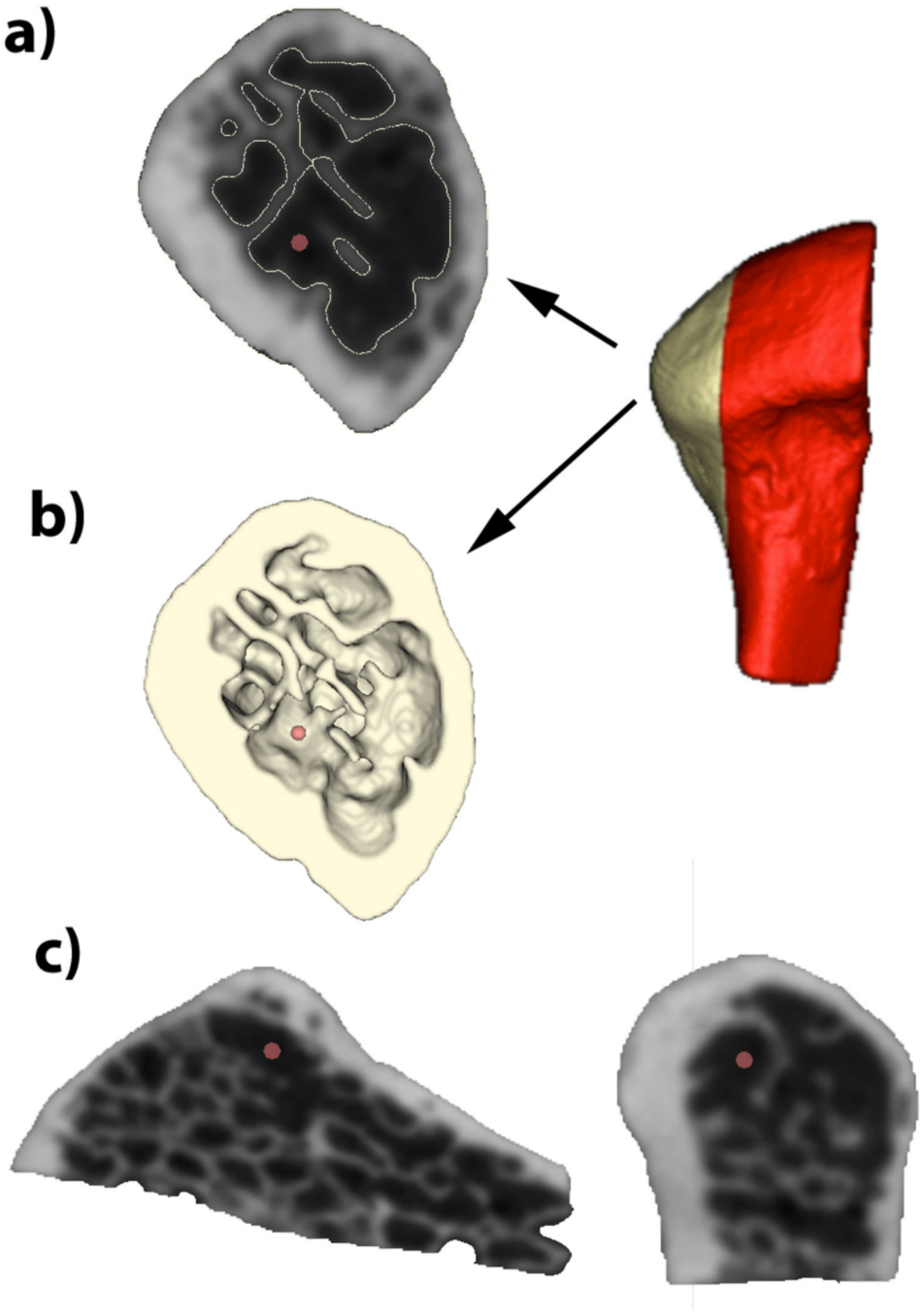

Figure 4.
Subchondral bone loss (red dot) in hr-CBCT a) sagittal + 3D reconstruction; b) axial and c) coronal views.

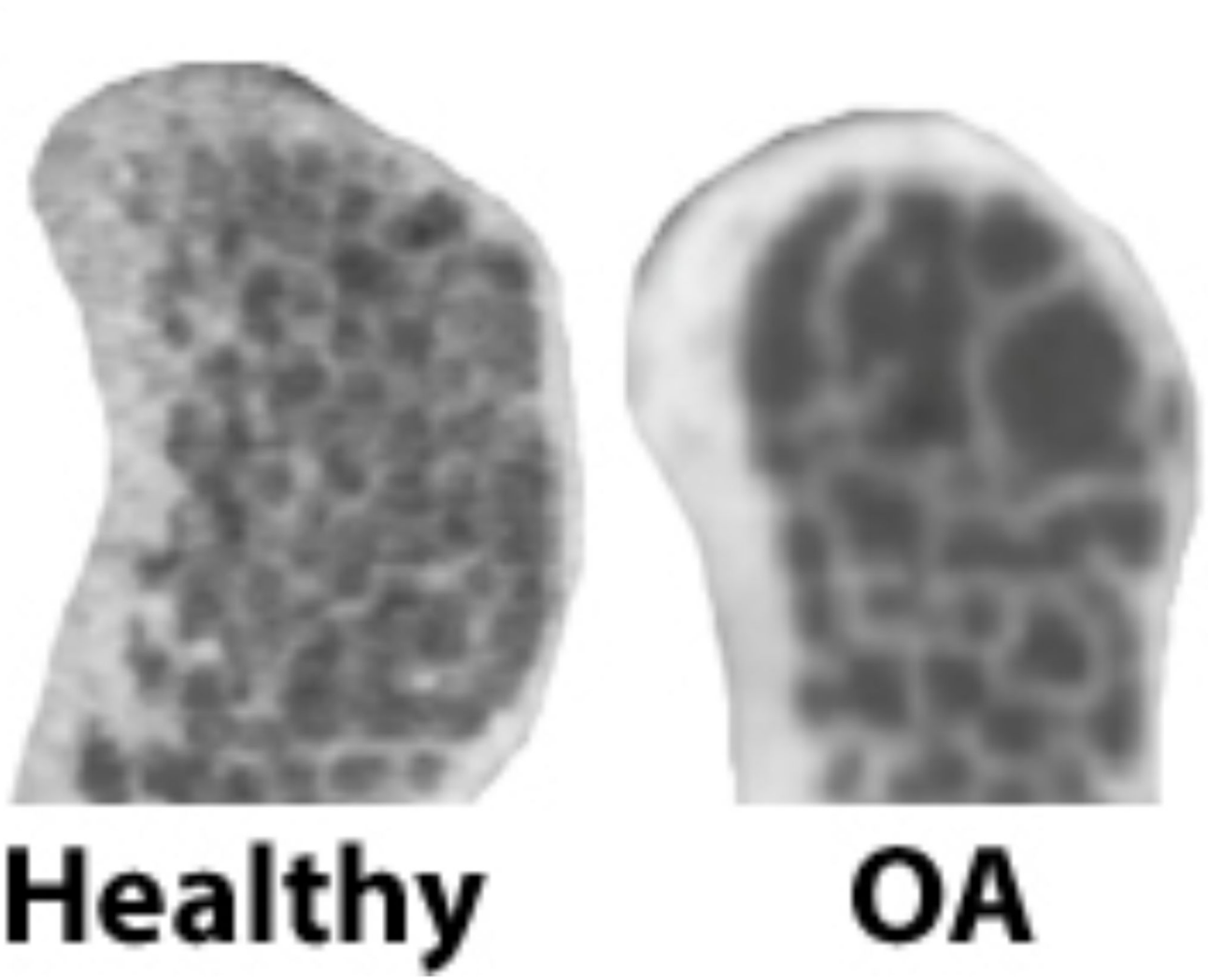

Figure 5.
Sagittal slices in a healthy and pathological TMJ condyle show clear qualitative differences due to OA

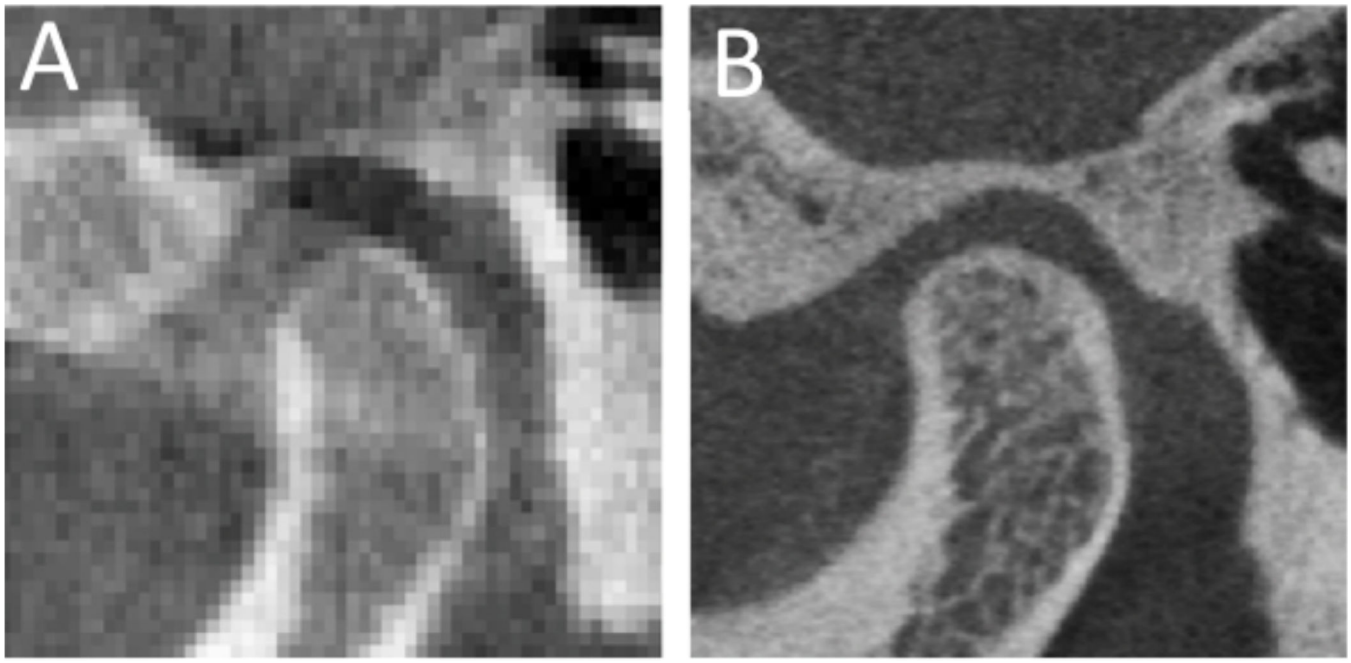

Figure 6.
Subchondral bone texture visualization in a sagittal slice of a) conventional CBCT and b) TMJ hr-CBCT protocol.

Table 1

Pearson's r correlation coefficient in co-occurrence textural features computed from μCT and hr-CBCT.

	Entropy	Energy	Contrast	Homogeneity
Pearson's r	0.50	**0.63**	**0.76**	0.48

Table 2

Pearson's r correlation coefficient in run-length textural features computed from μCT and hr-CBCT.

	SRE	LRE	GLN	RLN	RP
Pearson's r	−0.14	0.11	**0.84**	**0.77**	0.04